Electronic Supplementary Material (ESI) for Nanoscale.

Supporting Information

How to choose a precursor for decomposition solution-phase synthesis: The case of iron nanoparticles

*David A. J. Herman, Soshan Cheong, Andrew J. McGrath, Benjamin F. P. McVey, Matthias Lein and Richard D. Tilley**

Supporting Information

Contents

Experimental Section

Preparation of iron/iron oxide core/shell nanoparticles:

All reagents were purchased from Sigma Aldrich and used as received without further purification. All reaction procedures were performed under standard Schlenk techniques. The iron precursors $[Fe(\eta^5\text{-}C_6H_3Me_4)_2]$ and $[Fe(\eta^5\text{-}C_5H_5)(\eta^5\text{-}C_6H_7)]$ were both prepared according to previously described literature methods.[1] Ferrocene $[Fe(\eta^5\text{-}C_5H_5)_2]$ was purchased from Sigma Aldrich.

For the synthesis of iron nanoparticles (NPs), 0.31 mmol of iron precursor, oleylamine (7.5 mmol) and 1-octadecene (ODE) (1.5 mL) were degassed via freeze-pump-thaw (FPT) methods while separately ODE (8 mL) was degassed via FPT methods in a 3-necked flask then heated to 300°C, where the mixture containing the precursor was injected instantly. The reaction was left stirring at 300°C for 120 min then cooled to room temperature before being exposed to air and the iron NPs were purified via magnetic separation and redispersed in toluene for TEM analysis.

Physical Characterization

Transmission electron microscopy (TEM) images were taken on a JEOL 2010 TEM microscope at an acceleration voltage of 200 keV. Powder XRD measurements were obtained from a Pan Analytical X'pert Pro MPD X-ray diffraction System using Cu Kα radiation. Magnetization measurements were obtained from a dried iron NP sample, pressed and secured in a cylindrical gelatin holder and performed on a Quantum Design MPMS 2 SQUID magnetometer. Measurements were made using a Quantum Design MPMS 2 SQUID magnetometer. The variation of the magnetic moment was carried out by altering the applied field from 60,000 Oe (6 T) to -60,000 Oe (-6 T) at 300 K. The diamagnetic contribution of the gelatin capsule was corrected for by subtracting from the data sets the magnetic moment measured for the empty gelatin capsule and sample holder, but considered negligible due to the high magnetization values obtained from the NPs measured. UV/vis measurements were performed on an Agilent Diode Array Spectrometer 8453.

Computational Calculations

All calculations employed Density Functional Theory (DFT) in the form of the B3LYP hybrid-functional,[2] with the TZVP basis set of triple-ζ quality.[3] Molecules were optimized without symmetry constraints. Harmonic vibrational frequencies were calculated and all structures were determined to be minima on the potential energy surface. All calculations were performed using the Gaussian 09 Revision B.01 program[4].

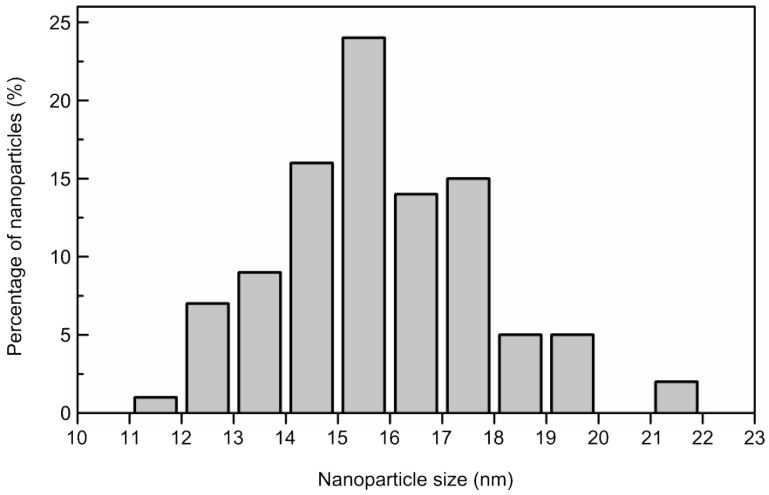

Figure S1. Size distribution of the iron/iron oxide core/shell nanoparticles synthesized via hot-injection at 300°C using bis(1,3,5-*exo*-6-tetramethyl-η^5-cyclohexadienyl)iron, [Fe(η^5-$C_6H_3Me_4)_2$]. The average nanoparticle size was 15.8 ± 1.6 nm.

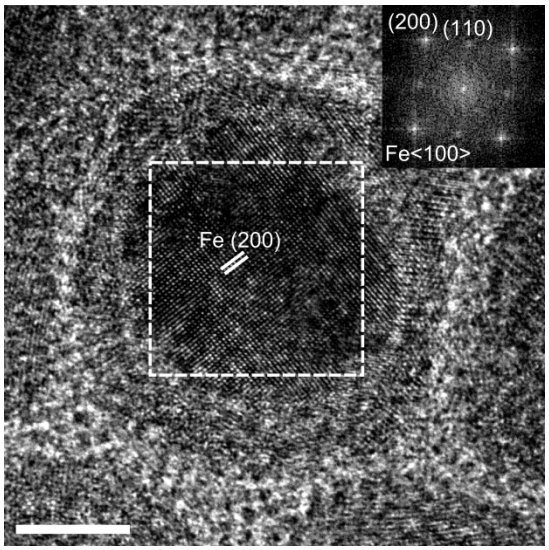

Figure S2. HRTEM image of the iron NPs synthesized via the decomposition of [Fe(η^5-$C_6H_3Me_4)_2$]. The darker core is single crystal α-Fe with lattice spacing's corresponding to Fe(200) planes. The lighter contrast shell is polycrystalline iron oxide with multiple planes observed in sections of the shell. Inset shows the corresponding FFT of the α-Fe core area in white dashed box viewed down the Fe <100> zone axis

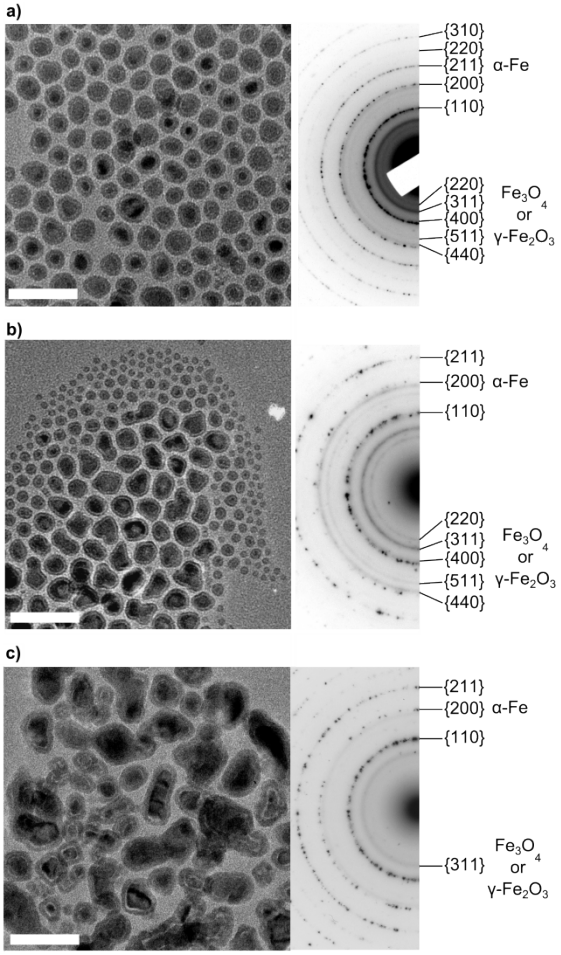

Figure S3. TEM images and corresponding selected area electron diffractions (SAED) of the iron NPs synthesized from a) $[Fe(\eta^5\text{-}C_6H_3Me_4)_2]$, b) $[Fe(\eta^5\text{-}C_5H_5)(\eta^5\text{-}C_6H_7)]$ and c) $[Fe(\eta^5\text{-}C_5H_5)_2]$

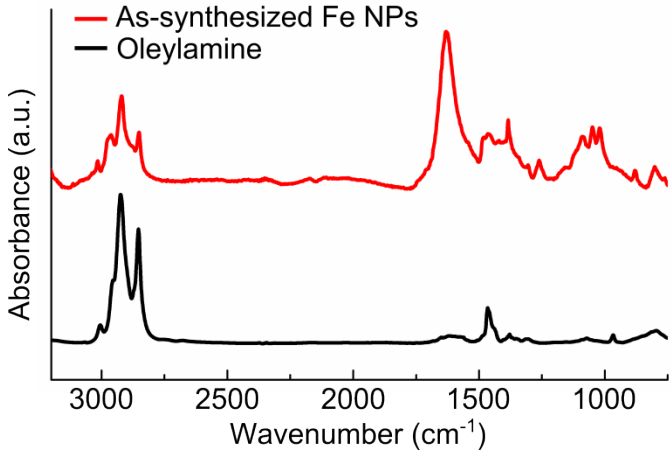

Figure S4: The IR peak positions (in cm^{-1}) for oleylamine are assigned as: 3005, ν (C=C-H); 2925, ν_{as} (CH_2); 2852, ν_s (CH_2); 1618, ν (C=C); 1466, δ_{as} (CH_2). These peaks are visible on the IR spectrum of the as-synthesized Fe NPs. The strong absorption band at 1620 cm^{-1} corresponds to chemisorbed atmospheric water on the surface of the washed Fe NPs.

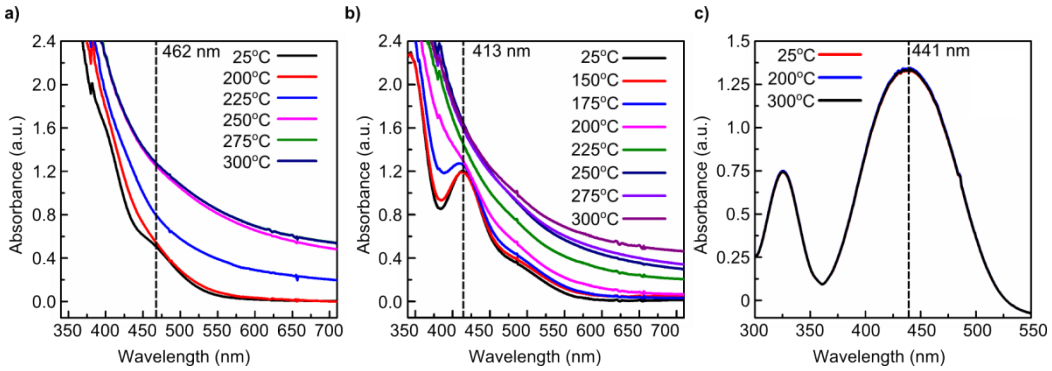

Figure S5. UV-Vis absorbance spectra monitoring precursor decomposition of a) $[Fe(\eta^5\text{-}C_6H_3Me_4)_2]$, b) $[Fe(\eta^5\text{-}C_5H_5)(\eta^5\text{-}C_6H_7)]$ and c) $[Fe(\eta^5\text{-}C_5H_5)_2]$ as a function of reaction temperature.

UV-Vis spectroscopy was performed on the precursors to monitor their decomposition. 0.31 mmol of iron precursor was suspended in a mixture of oleylamine (7.5mmol) and octadecene (9.5 mL) and heated from room temperature to 300°C, with reaction aliquots being removed every 25°C, quenched in an ice-bath to arrest any further precursor decomposition and suspended in cyclohexane. Precursor decomposition is observed to occur when the intensity of the peak of interest increases, which is indicative of the formation of small Fe clusters and nuclei resulting in the solution becoming too opaque to measure absorption as a result of scattering.

For the decomposition of a) $[Fe(\eta^5\text{-}C_6H_3Me_4)_2]$, reaction aliquots taken from 25 – 200°C resulted in no obvious change in absorbance with a shoulder observed at 462 nm. Aliquots taken from 225 – 300°C resulted in a sharp increase in intensity at 462 nm. For b) $[Fe(\eta^5\text{-}C_5H_5)(\eta^5\text{-}C_6H_7)]$, reaction aliquots taken from 25 – 150°C resulted in no obvious change in absorbance at 413 nm. Aliquots taken from 150 – 225C resulted in a gradual change in intensity at 413nm, plateauing off at 225 – 300°C. For c) $[Fe(\eta^5\text{-}C_5H_5)_2]$, no observable change in peak intensity at 441 nm is observed between 25-300°C indicating minimal precursor decomposition.

Table S1. Computational calculations of bond dissociation energies (BDE) of ligands from the respective precursors Fe(II) centers. Below, molecular structures of the precursors resolved from the computational calculations, from left to right, a) $[Fe(\eta^5\text{-}C_6H_3Me_4)_2]$, b) $[Fe(\eta^5\text{-}C_5H_5)(\eta^5\text{-}C_6H_7)]$ and c) $[Fe(\eta^5\text{-}C_5H_5)_2]$.

Reaction	ΔE (kJ.mol^{-1})
a) $Fe(\eta^5\text{-}C_6H_3(Me)_4)_2 \rightarrow Fe(\eta^5\text{-}C_6H_3Me_4)^+ + C_6H_3Me_4^-$	-199.4
b) $Fe(\eta^5\text{-}C_5H_5)(\eta^5\text{-}C_6H_7) \rightarrow Fe(\eta^5\text{-}C_5H_5)^+ + C_6H_7^-$	-233.5
$Fe(\eta^5\text{-}C_5H_5)(\eta^5\text{-}C_6H_7) \rightarrow Fe(\eta^5\text{-}C_6H_7)^+ + C_5H_5^-$	-209.4
c) $Fe(\eta^5\text{-}C_5H_5)_2 \rightarrow Fe(\eta^5\text{-}C_5H_5)^+ + C_5H_5^-$	-224.6

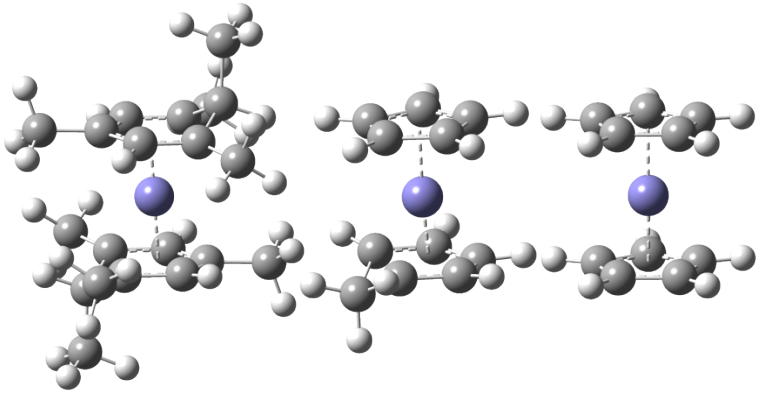

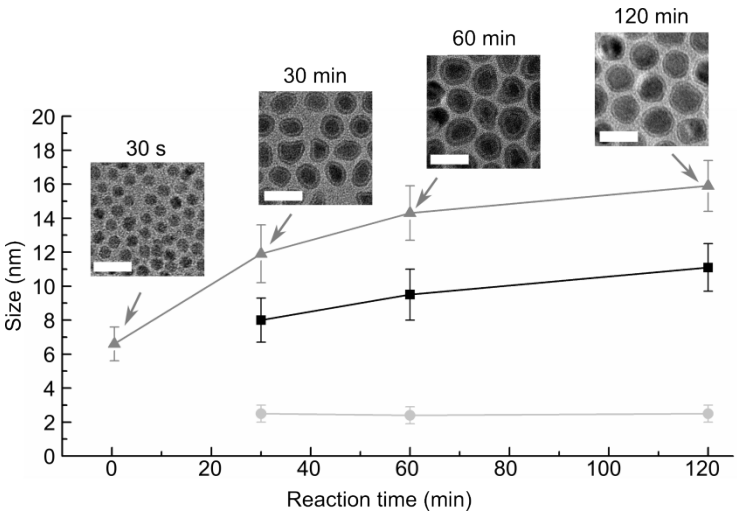

Figure S6. Overall nanoparticle (grey), iron core diameter (black) and iron oxide shell width (light grey) versus reaction time (min) of iron NPs synthesized from [Fe(η^5-$C_6H_3Me_4)_2$]. Time-resolved samples were obtained by performing 5 different reactions with reaction times of 0.5, 30, 60 and 120 min. (Standard size deviation is shown as error bars. Representative TEM images of each sample are shown in A-D). Scale bars: 20 nm

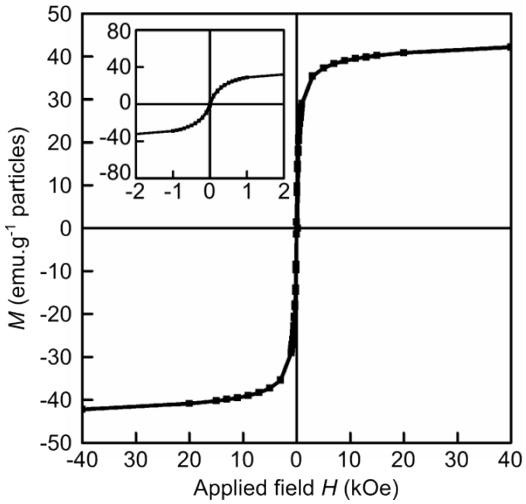

Figure S7. Room temperature magnetization curve of the iron oxide NPs synthesized after 30 s using [Fe(η^5-$C_6H_3Me_4)_2$]. Inset shows the low field regions with the curve intercepting at the origin, indicating the absence of remnant magnetization or coercivity indicating superparamagnetic behavior

1 (a) M. D. Clerk, M. J. Zaworotko, B. Borecka, T. S. Cameron, D. L. Hooper and A. Linden, *Can. J. Chem.*, 1990, **68**, 1823-1931; (b) M. L. H. Green, L. Pratt and G. Wilkinson, *Journal of the Chemical Society (Resumed)*, 1960, 989-997.

2 (a) A. D. Becke, *J. Chem. Phys*,. 1993, **98**, 5648; (b) C. Lee, W. Yang and R. G. Parr, *Phys. Rev. B.*, 1988, **37**, 785; S. H. Vosko, L. Wilk and M. Nusair, *Can. J. Phys.*, 1980, **56**, 1200; P. J. Stevens, F. J. Devlin, C. F. Chabalowski and M. J. Frisch, *J. Phys. Chem.* 1994, **98**, 11623.

3 F. Weigend and R. Ahlrichs, *Phys. Chem. Chem. Phys.*, 2005, **7**, 3297.

4 M. J. Frisch, G. W. Trucks, H. B. Schlegel, G. E. Scuseria, M. A. Robb, J. R. Cheeseman, G. Scalmani, V. Barone, B. Mennucci, G. A. Petersson, H. Nakatsuji, M. Caricato, X. Li, H. P. Hratchian, A. F. Izmaylov, J. Bloino, G. Zheng, J. L. Sonnenberg, M. Hada, M. Ehara, K. Toyota, R. Fukuda, J. Hasegawa, M. Ishida, T. Nakajima, Y. Honda, O. Kitao, H. Nakai, T. Vreven, J. A. Montgomery, Jr., J. E. Peralta, F. Ogliaro, M. Bearpark, J. J. Heyd, E. Brothers, K. N. Kudin, V. N. Staroverov, T. Keith, R. Kobayashi, J. Normand, K. Raghavachari, A. Rendell, J. C. Burant, S. S. Iyengar, J. Tomasi, M. Cossi, N. Rega, J. M. Millam, M. Klene, J. E. Knox, J. B. Cross, V. Bakken, C. Adamo, J. Jaramillo, R. Gomperts, R. E. Stratmann, O. Yazyev, A. J. Austin, R. Cammi, C. Pomelli, J. W. Ochterski, R. L. Martin, K. Morokuma, V. G. Zakrzewski, G. A. Voth, P. Salvador, J. J. Dannenberg, S. Dapprich, A. D. Daniels, O. Farkas, J. B. Foresman, J. V. Ortiz, J. Cioslowski and D. J. Fox, Gaussian 09 (Revision B.01), Gaussian Inc., Wallingford, CT, 2009.

5 Spectrometric Identification of Organic Compounds R. M. Silverstein, F. X. Webster, D. J. Kiemle, John Wiley & Sons Inc., 2005.